AN EXPERIMENTAL STUDY OF THE BEHAVIOR OF INTUMESCENT COATINGS UNDER LOCALIZED FIRES

AN EXPERIMENTAL STUDY OF THE BEHAVIOR OF INTUMESCENT COATINGS UNDER LOCALIZED FIRES

Qing Xu[1], Guo-Qiang Li[1, 2*], Yong C. Wang[3], Luke Bisby [4]

[1] College of Civil Engineering, Tongji University, Shanghai 200092, China

[2] State Key Laboratory for Disaster Reduction in Civil Engineering, Tongji University, Shanghai 200092, China

[3] School of Mechanical, Aerospace and Civil Engineering, University of Manchester, UK

[4] School of Engineering, University of Edinburgh, UK

Abstract

This paper presents an experimental study of the behavior of intumescent coatings exposed to localized fires. The main objective is to assess the extent to which thermal properties of intumescent coatings obtained under uniform heating can be applied for localized fire exposures. The experiments used two types of specimens representing protected steel beams and columns. Localized pool fires were placed underneath horizontal specimens or beside vertical specimens. Solvent-based and waterborne intumescent coatings were applied to the specimens. Measurements were made of temperatures of the steel specimens and the adjacent gas phase, as was coating expanded thicknesses at several locations. Depending on their location relative to fires, the intumescent coatings were variably unreacted, melted, partially expanded, or fully expanded (corresponding to steel temperatures of about less than 100℃, 100-300℃, 300-400℃, and above 400℃, respectively). The appearances and expansion ratios for various regions of coatings under localized fires were consistent with those under uniform heating from previously obtained furnace test results. Steel temperatures of the specimens were calculated using thermal conductivities of coatings derived from furnace tests, and were found to agree reasonably with the experimental results, thus indicating that it may be feasible to apply thermal conductivities derived from furnace tests to predict steel temperatures under localized heating scenarios.

* Corresponding author: gqli@tongji.edu.cn

Keywords: intumescent coating; reactive region; steel temperature; expansion ratio; effective constant thermal conductivity; localized heating

1. INTRODUCTION

In fire resistance design of building structures, the temperature-time relationship of the fire is typically assumed to be uniform and is intended to reflect a post-flashover condition within a fire compartment. This uniform temperature-time relationship is typically assumed to follow the ISO 834 standard temperature-time curve [1], or similar idealized curves such as the parametric fire curves in EN 1991-1-2 Annex A [1]. However, real fire exposures are likely to result in non-uniform thermal exposures, particularly in larger spaces; assuming a uniform thermal exposure is therefore not always suitable [2]. Various research studies have investigated how to quantify non-uniform temperature distributions or heat fluxes experienced under localized fires (Wakamatsu [3,4], Ferraz [5], Bystrom [6], Hanus [7], NIST [8] and Tondini [9]). However, there is a paucity of experiments on the response of intumescent-protected steel structures subjected to localized fires.

Intumescent coatings are widely used to protect steel structures against fire due to advantages such as lightweight, attractiveness, and suitability for on- and off-site application. Intumescent coatings expand under severe heating to form a protective char layer which can provide thermal insulation in a fire [10]. The chemical reactions within intumescent coatings are complex, with variable expansions and effective thermal conductivities displayed under different heating regimes.

To date, most research studies on intumescent coatings have focused on their expansion and thermal properties under spatially uniform heating; this includes the ISO 834 standard furnace test condition as well as other, non-standard but uniform, fires. Li [11,12] proposed the constant effective thermal conductivity concept for ISO 834 fire conditions, as well as a three-stage effective thermal conductivity [13] model for non-standard uniform furnace test conditions as a simplification for the temperature-dependent effective thermal conductivity method suggested in EN 13381-8 [14]. In the

three-stage model, the behavior of intumescent coatings is divided into three stages: (1) melting, (2) expanding, and (3) fully expanded, when the steel temperatures are in the ranges of about 100℃-300℃, 300℃-400℃, and higher than 400ºC, respectively. The applicability of the three-stage thermal conductivity method for intumescent coatings under uniform, non-standard, large space fires has been demonstrated under some conditions [13]. Studies by Wang [15], Elliott [16], Lucherini [17], and de Silva [18, 19] have also been limited to intumescent coatings under spatially uniform fire conditions.

However, since the behavior of intumescent coatings depends on the fire conditions, it is necessary to investigate whether the response of intumescent coatings under uniform heating can be reasonably applied to cases of non-uniform heating.

This paper presents the results of a series of pool fire experiments on intumescent coating protected real-scale steel specimens. The experiments were carried out on horizontal and vertical steel members under different localized fire scenarios. The main objective of the study was to compare the behavior of intumescent coatings under localized fires against that under spatially uniform heating in furnace tests, as well as to assess whether the effective thermal properties of intumescent coatings derived on the basis of furnace testing can reasonably be used to predict the temperature of protected steelwork under localized fire exposures.

2. TEST SPECIMENS

2.1 Steel members

Square hollow steel tubes with dimensions of 250×250×8mm were used for all experiments. The section factor of the sections used was 132.98m^{-1}. Prior studies have shown that the shape of steel sections had little influence on intumescent coating behavior [18] except for possible cracking and stickability issues. The two horizontal experimental specimens were each 5m in length, and the four vertical specimens were 4m in height. The specimens were unloaded with welded end plates added for stability during testing.

2.2 Thermocouples

The steel temperatures and surrounding gas temperatures were measured by Type-K inconel sheathing thermocouples with a diameter of 2mm at selected locations. Figure 1 shows the locations of thermocouples installed at eleven cross-sections along the horizontal members, and Figure 2 shows the eight cross-sections in the vertical members. These cross-sections of thermocouples allowed detailed measurement of temperatures under the experimental heating conditions. Due to large temperature gradients close to the fire source, the thermocouple locations near the specimen centers, where the fire source was located for horizontal specimens, were more closely spaced.

At each cross-section eight thermocouples were installed. As shown in Figure 3, four of these were embedded (with an embedment depth of 4mm) in the steel cross-section to measure steel temperatures. This method of thermocouple installation was chosen to ensure that the thermocouples stayed in place and to avoid any disturbance to intumescent coatings. The other four thermocouples were located approximately 70mm from the steel surface to measure the surrounding gas phase

temperatures. The thermocouples measuring steel temperatures were denoted “TS-section number-surface name” and those measuring gas temperatures were “TG- section number- surface name”. The steel surfaces refer to the front surface facing the fire (F), the back surface (B) and the two side surfaces (S1, S2).

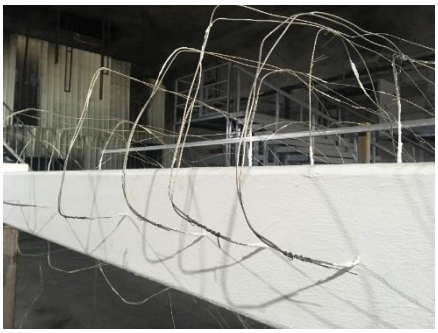

(a) Thermocouples on a horizontal (beam) specimen

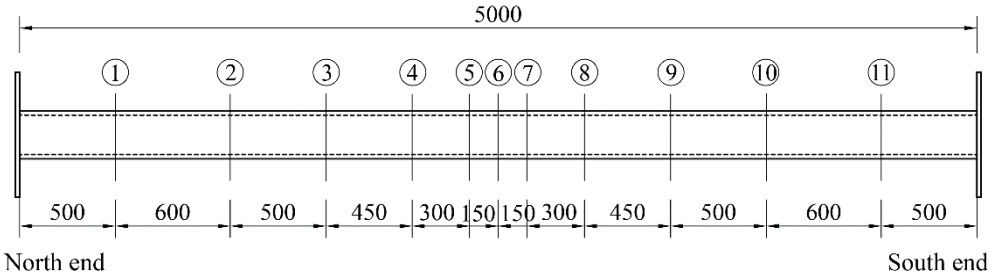

(b) Thermocouple stations along horizontal specimens

Figure 1 Thermocouple locations for horizontal specimens (Units: mm)

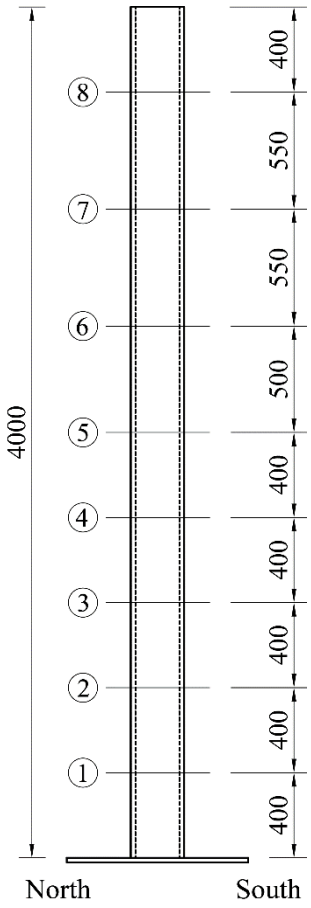

Figure 2 Thermocouple stations for vertical specimens (Units: mm)

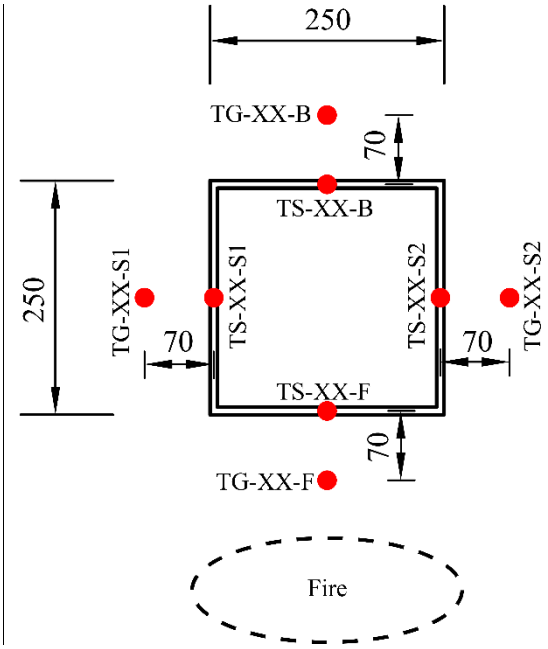

(TG- Thermocouples for gas temperature; TS- Thermocouples for steel temperature (Units: mm))

Figure 3 Locations of thermocouples at each cross-section

2.3 Fire protection

Two types of commercial intumescent coatings were applied to the specimens: a single component waterborne intumescent coating, and a single component solvent-based acrylic intumescent coating. The target dry film thickness (DFT) for both types of intumescent coatings was 0.6mm on all specimens. This DFT is typical of that required to achieve a standard fire resistance rating of 30min for the coatings used for a steel limiting temperature of 500ºC. The duration of pool fire tests of this study was also approximately 30 minutes. The actual installed DFT of the intumescent coatings was measured at 150 locations for each specimen, and the average value was taken as the measured DFT for the specimen. The measured values of intumescent coating thickness were within ±10% of the average DFT value. Table 1 provides a summary of the test specimens.

Table 1 Summary of test specimens

Specimen No.	Specimen type	Length (m)	Coating type	Number of cross-sections for temperature measurement	Average coating DFT/ (μm)	Standard deviation of DFT/ (μm)
BW	Horizontal	5	Waterborne	11	613	65
BS	Horizontal	5	Solvent-based	11	660	54
CW1/CW2	Vertical	4	Waterborne	8	691/677	64/61
CS1/CS2	Vertical	4	Solvent-based	8	655/680	51/55

3. FIRE EXPOSURE

3.1 Fire source

Pool fires were used in the tests to simulate localized fires. The burner metal box was square measuring 1m by 1m in plan and 0.2m in depth, equivalent to a circular fire source with a diameter

of 1.13m in terms of the surface area. N-heptane was used as fuel because of its high calorific value and low smoke density. The burning duration of a pool fire in the open can be estimated by Eqn. (1) [20]:

$$t_b = \frac{4V}{\pi D^2 v} \tag{1}$$

Where V is the volume of the fuel (m^3); D is the diameter of the pool (m) and v is the rate of fuel consumption (m/s), which is defined in Eqn. (2):

$$v = \frac{\dot{m}''}{\rho} \tag{2}$$

$$\dot{m}'' = \dot{m}''_{\infty}(1 - \exp(-k\beta D)) \tag{3}$$

where $\dot{m}''$ is the estimated burning rate; ρ is the fuel density (kg/m^3); $\dot{m}''_{\infty}$ is taken as 0.101 $kg/m^2 \cdot s$ and $k\beta$ is 1.1 m^{-1} for Heptane [20].

The fires were designed to achieve a heat release rate (HRR) of approximately 2MW and a steady burning duration of about 30 minutes. HRR can be related to the mass loss rate according to Eqn. (4):

$$\dot{Q}(t) = \dot{m}(t)\chi_{eff}\Delta H_c \tag{4}$$

where ΔH_c is the heat of combustion and χ_{eff} the combustion efficiency (assumed as 0.8 [21]). The heat of combustion of heptane is 44.6 MJ/kg [22]. Thus, to achieve an HRR of 2MW the estimated mass loss rate, $\dot{m}(t)$, is approximately 0.072 kg/s; this can be provided by an N-heptane pool fire with a diameter of 1.13m (see Equation (4)). Finally, to achieve a burning time of 30 minutes a fuel depth of 14cm was used (see Equation (1)).

Table 2 provides details of the measured burning time, the estimated and the average measured heat release rates for all the tests.

Table 2 Summary of fire exposure for different tests

Test No.	Specimen No.	Specimen Type	Fuel Volume (L)	Duration (min)	Estimated HRR (MW)	Measured average HRR (MW)
1	BW	Horizontal	140	27.5	2.57	2.07
2	BS	Horizontal	140	27.5	2.57	2.07
3	CS1, CW2	Vertical	130	24.2	2.57	2.18
4	CW1, CS2	Vertical	135	25.5	2.57	2.15

3.2 Fire locations

The fire tests were conducted in a seven-metre high testing hall. The horizontal specimen was simply-supported on two steel stubs, as shown in Figure 4. The pool fire was located beneath mid-span of the specimen at one meter below its lower flange. For the vertical specimens, two specimens were fixed to the ground and placed adjacent to the fire pool, as shown in Figure 5.

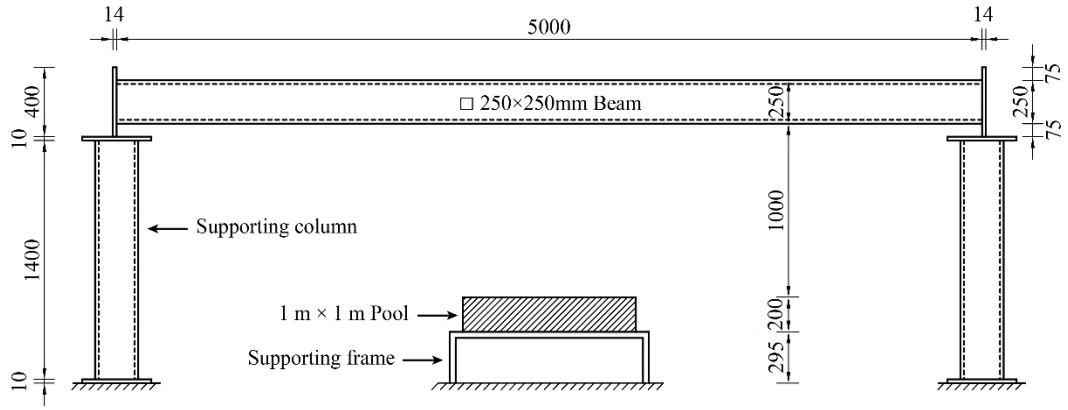

(a) Test setup (Units: mm)

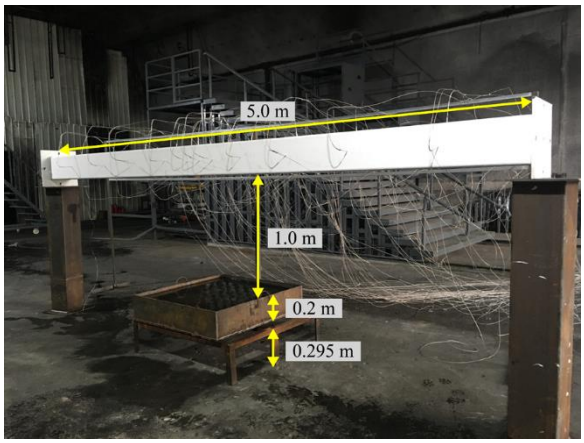

(b) Test specimen before fire testing

Figure 4 Test setup for horizontal specimens

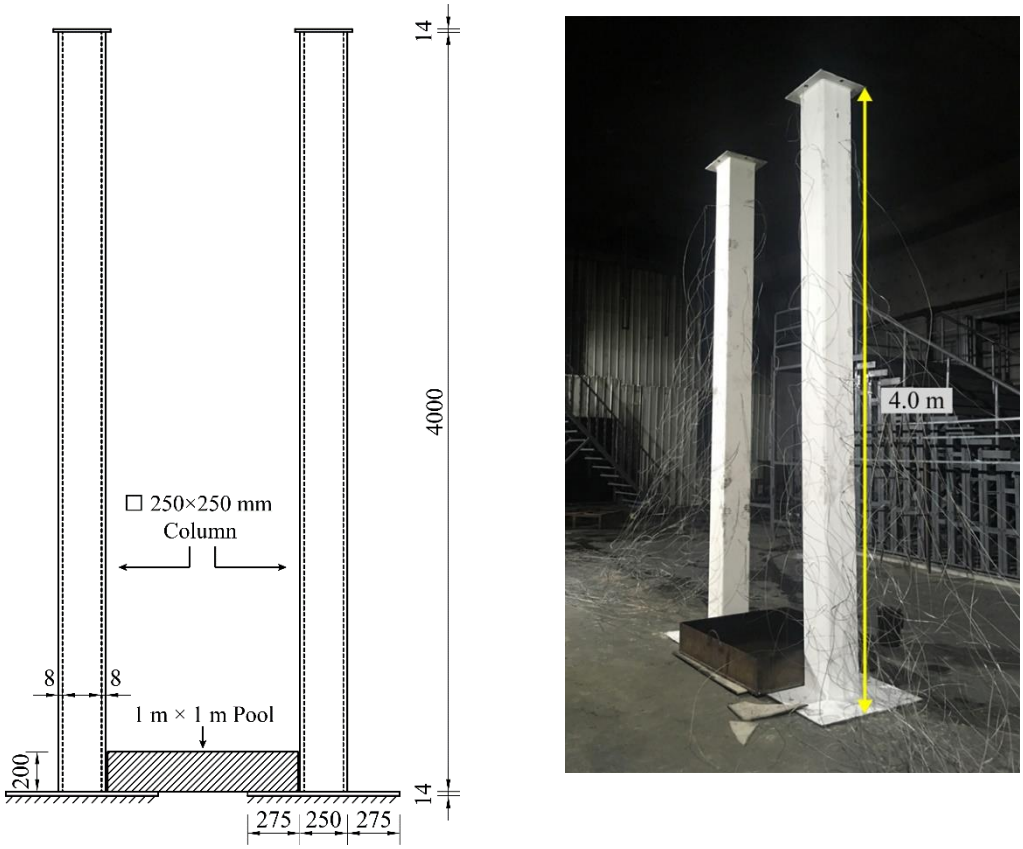

(a) Test setup (b) Specimens before test

Figure 5 Test setup for vertical specimens (Unidentified units: mm)

3.3 Flame observation

Figure 6 shows typical horizontal and vertical tests in progress. According to [22], the flame height L_f can be calculated using the following equation:

$$L_f = -1.02D + 0.235\dot{Q}^{2/5} \tag{5}$$

where L_f and D are in m and $\dot{Q}$ is in kW. Substituting a value of D=1.13 m and $\dot{Q}$ =2.07 MW in the above equation gives a value of 3.82 m for the flame height, which agrees reasonably well with the observed flame heights between 3.5 and 4 m.

It can be seen in Figure 6 that the flame slightly swayed to the north during the tests, which was due to the ventilation conditions in the laboratory. The north sway of the flame resulted in different thermal conditions for the north and south columns tested in the vertical orientation, with

the north column effectively engulfed within the fire plume and the south column somewhat removed from the flames.

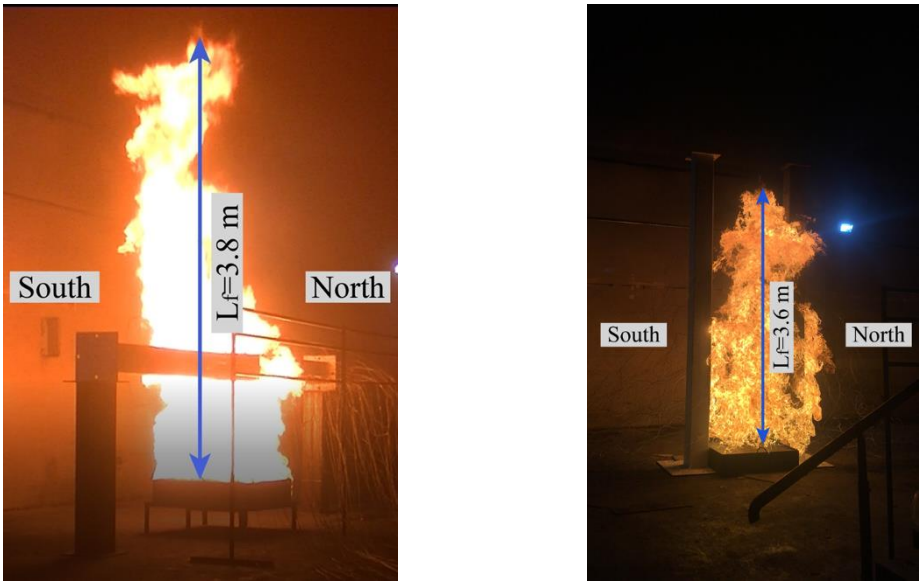

(a) Horizontal test (b) Vertical test

Figure 6 Tests in progress

3.4 Fire temperature distributions

The gas temperatures for the beam and column specimens were highly non-uniformly distributed and fluctuated considerably; this is shown in Figure 7 and Figure 8, which show a selection of measured gas temperature-time relations for the different horizontal and vertical specimens. Due to the ventilation conditions inside the test lab, the flame tilted to the north. As a result, the gas temperatures for south sections 5-8 of the horizontal specimens decreased at about 500s, while those for the north sections (9-11) increased. Similarly, the flame surrounded the north vertical specimen on all surfaces, but not the south specimen, so the gas temperatures on the side and back surfaces of the north specimen (CW1, CS1) were more than one hundred degrees higher than those of the south specimen (CW2, CS2).

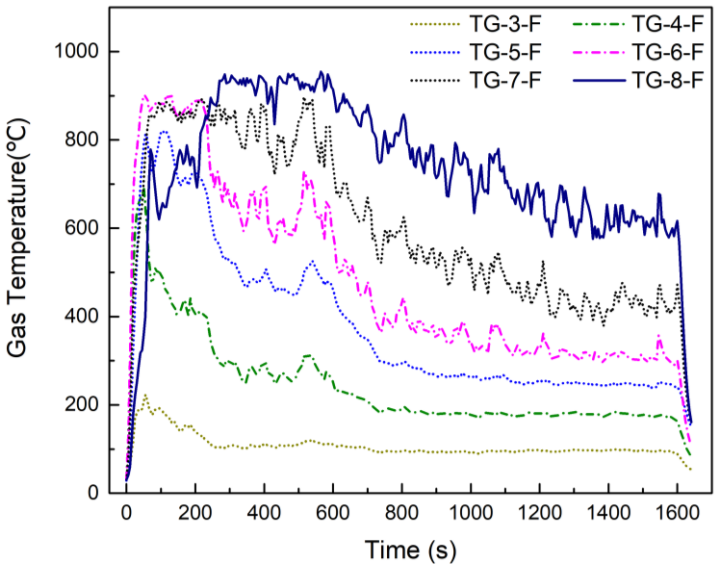

(a) Gas temperatures for sections 3-8

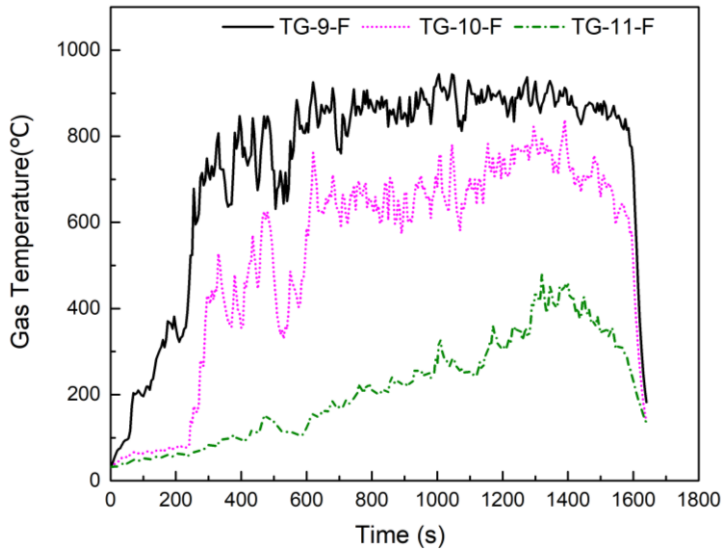

(b) Gas temperatures for sections 9-11

Figure 7 Selected gas temperatures at the front surface for horizontal member with waterborne intumescent coatings (BW)

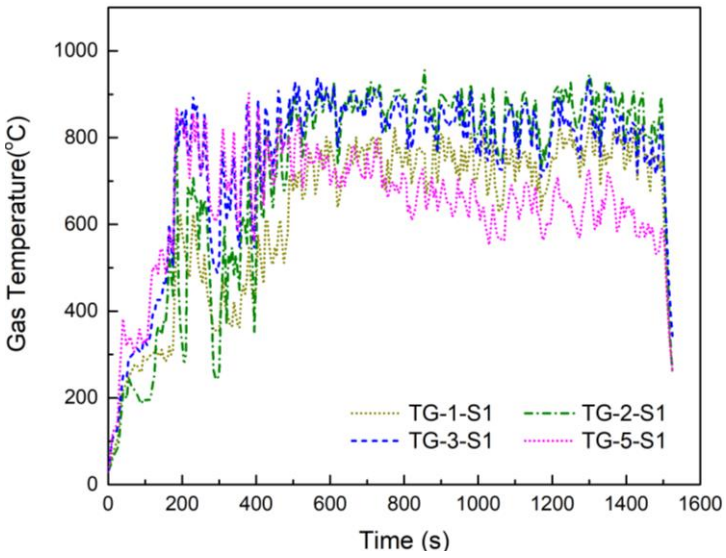

(a) Side surface of north column CW1

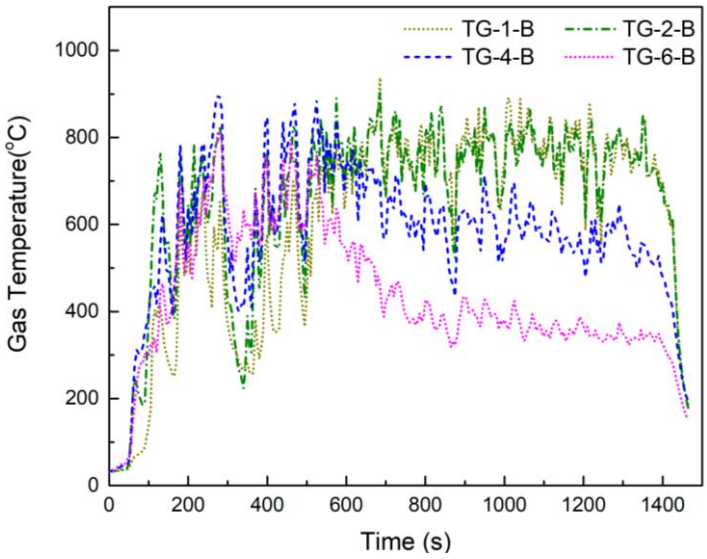

(b) Back surface of north column CS1

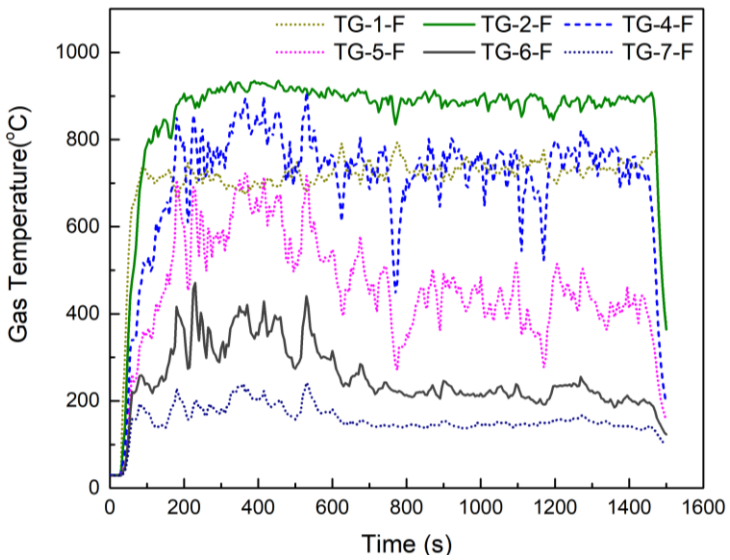

(c) Front surface of south column CW2

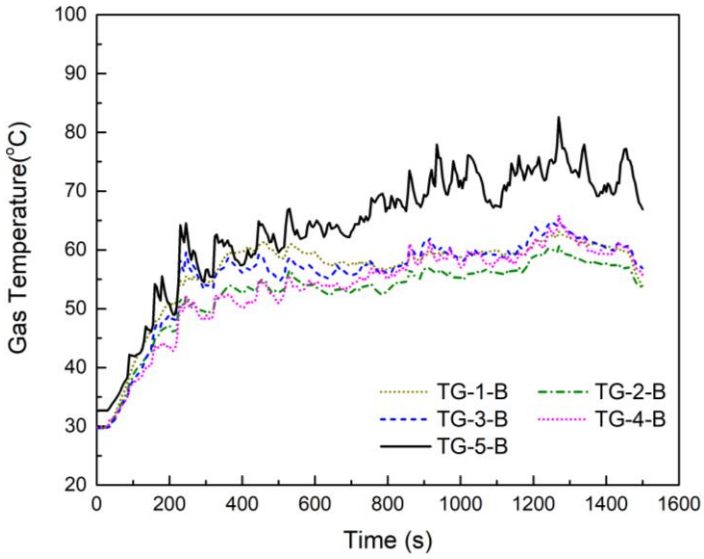

(d) Back surface of south column CW2

Figure 8 Selected gas temperatures for different vertical specimens with waterborne intumescent coatings

4. RESPONSE OF INTUMESCENT COATINGS

4.1 Reactions of intumescent coatings

Observations of intumescent coatings after the fire tests show four regions: 1 –fully expanded, 2 – partially expanded, 3 – melted but not expanded, and 4 – virgin material. The intumescent coating is considered “fully expanded” if its surface appearance after expansion is white, which indicates oxidation of the char, and bubbles were fine sized and reasonably uniformly distributed. Region 1 was directly engulfed in the fire plume, because the temperatures of intumescent coatings not engulfed in the fire plume were not sufficiently high (surrounding gas temperature > 600ºC) to allow the intumescent coatings to undergo the full chemical reactions for expansion. Region 2 experienced expansion but did not fully expand, because the temperatures were insufficient for full chemical reactions, as in Region 1. Within this region, the recorded gas temperatures were between 300-600°C. In this region, the char surfaces were black, suggesting the presence of carbon on the

char surface and an absence of significant char oxidation, with bubbles of different sizes within the coating. Region 3 (melting region) displayed a few very small bubbles scattered on the coating surface, but no obvious coating expansion. The nearby fire temperature was higher than the melting temperature of intumescent coatings (i.e. about 150°C [23]) but lower than the temperatures required for onset of expansion of about 300°C [23]. In Region 4 (essentially virgin material), the surrounding gas temperatures were low (<100°C) and there was no indication of any melting or gasification processes. The transition between different regions was smooth, without any obvious particularities between the regions, and so these can be delineated only approximately. Different sizes of bubbles were observed at different expansion regions, where the coatings were at different stages of expansion. No holes were observed in the surface of the intumescent coating.

Figure 9 and Figure 10 show typical surface appearances of these four regions for the waterborne and solvent-based intumescent coatings respectively. Figures 11, 12 and 13 show their distributions along the horizontal and vertical specimens. As shown in Figure 9, the effectively expanded intumescent coatings in Region 1 had a continuous, smooth char, with small and evenly distributed white bubbles on the surface. This is similar to observations of fully expanded intumescent coatings in ISO 834 standard furnace tests [12,13,24].

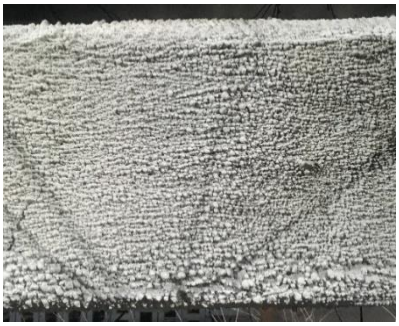

(a) Full expansion region (Region 1)

(b) Expanding region (Region 2)

(c) Melting region (Region 3)

(d) Virgin material (Region 4)

Figure 9 Typical surface appearances of four notional regions of waterborne intumescent coatings

(a) Full expansion region (Region 1)

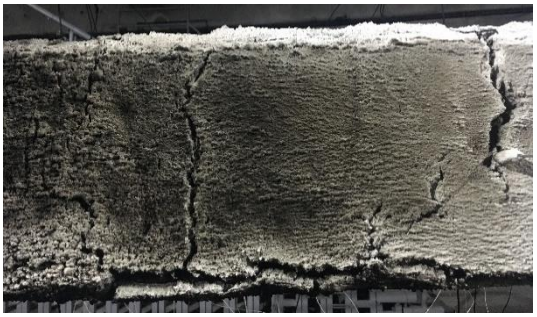

(b) Expanding region (Region 2)

(c) Melting region (Region 3)

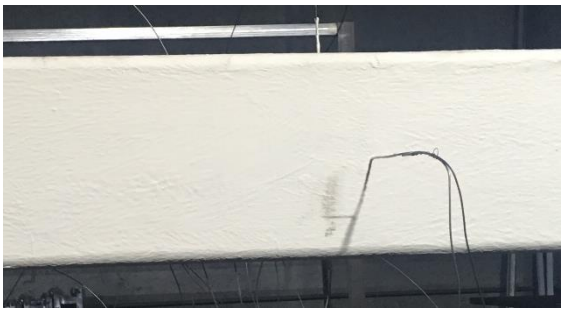

(d) Virgin material (Region 4)

Figure 10 Typical surface appearances of four notional regions of solvent-based intumescent coatings

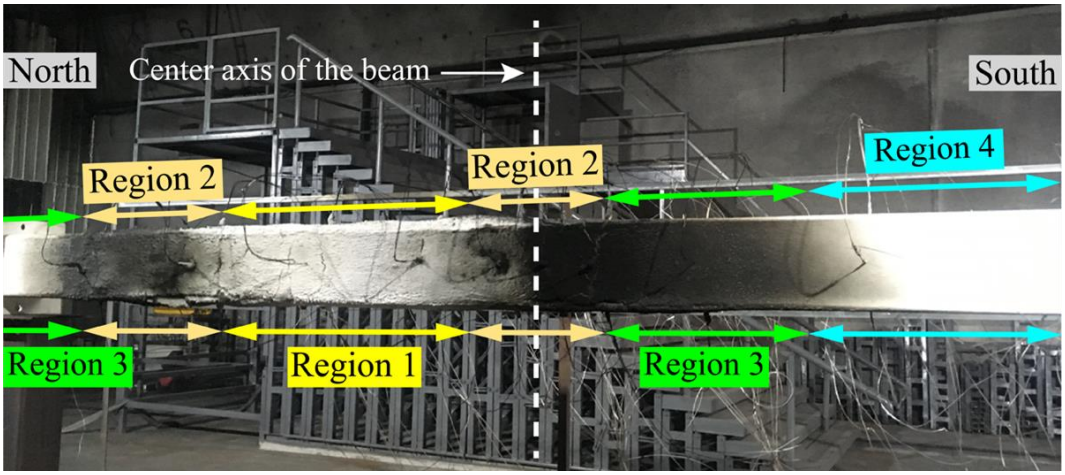

(a) Distribution of the four regions on horizontal specimen, side surface 1

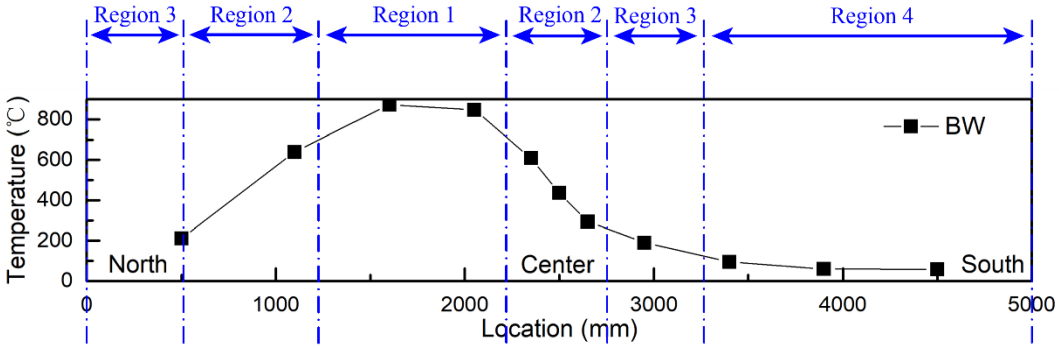

(b) Approximate gas temperature distribution during steady burning stage, side surface 1

Figure 11 Distribution of four notional regions for waterborne coating and relation to average gas phase temperature distribution

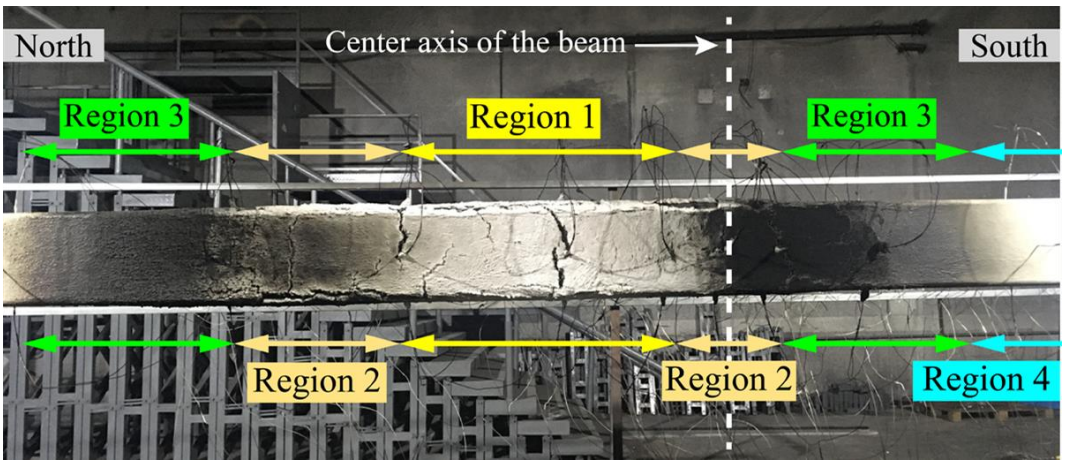

(a) Distribution of the four notional regions, side surface 1

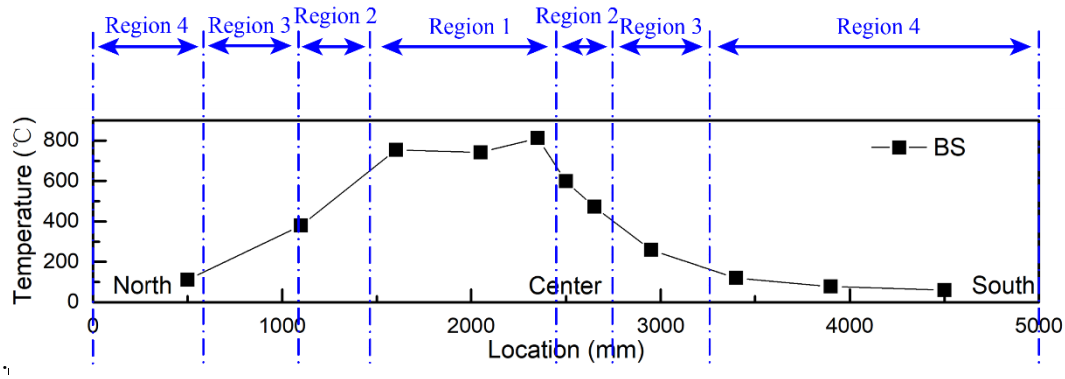

(b) Approximate gas temperature distribution during steady burning stage, side surface 1

Figure 12 Distribution of four notional regions for solvent-based coating on horizontal specimen, and relation to average gas phase temperature distribution

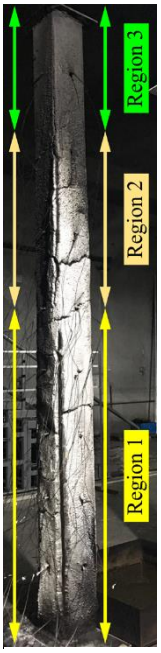

(a) CW1, side surface 1

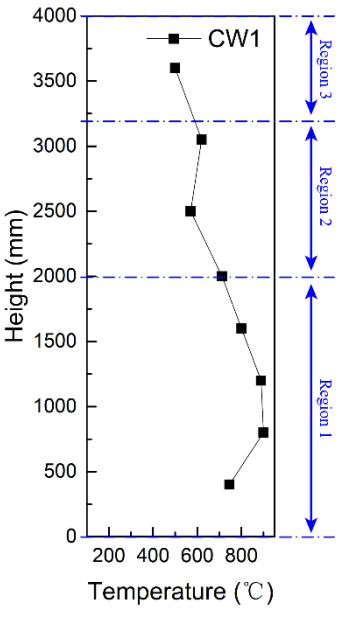

(b) Gas temperature distribution of CW1

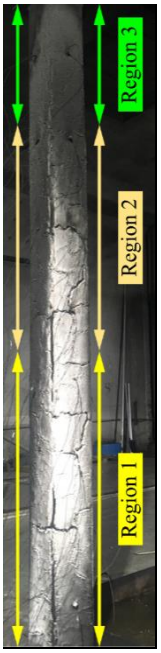

(c) CS1, side surface 1

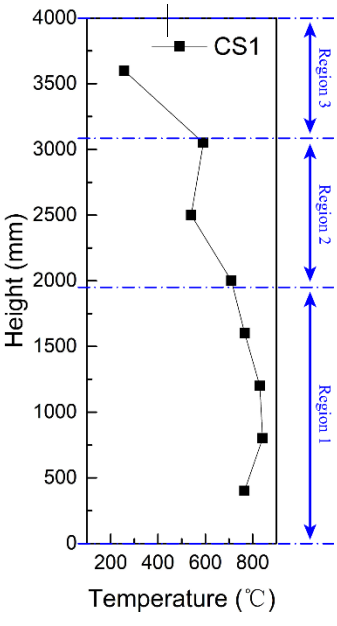

(d) Gas temperature distribution of CS1

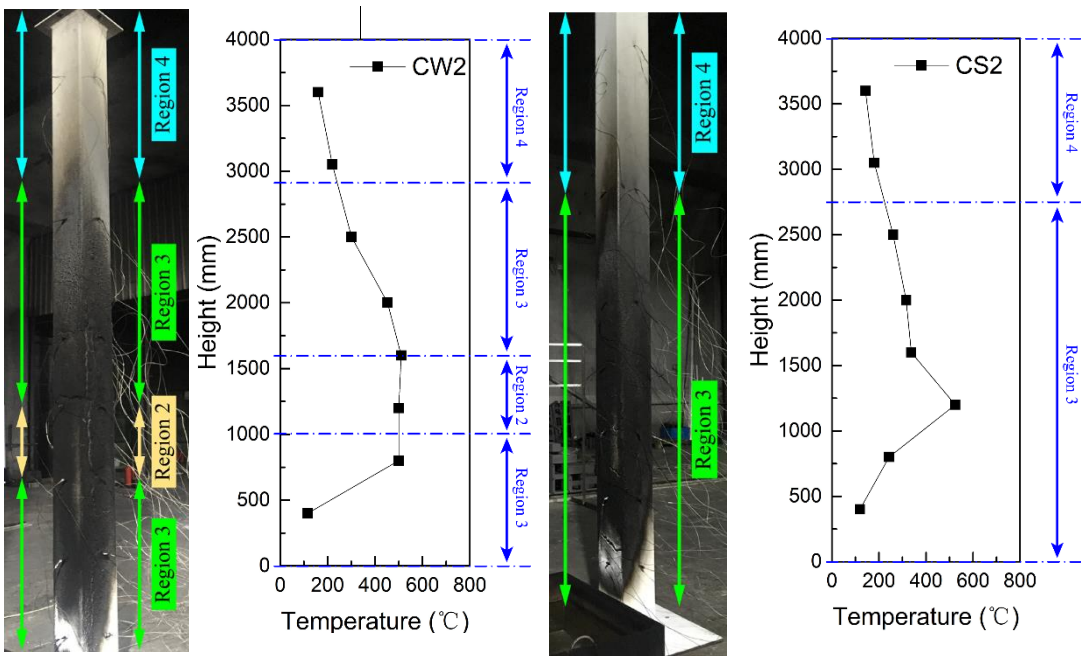

(e) CW2, side surface 1 (f) Gas temperature distribution of CW2 (g) CS2, side surface 1 (h) Gas temperature distribution of CS2

Figure13 Distribution of different notional regions of intumescent coatings along vertical members and relation to average gas phase temperature distribution

Figure 13 shows that intumescent coatings on the two north columns (CS1 and CW1) reacted more fully (white char) than the two south columns (black char) due to higher gas temperatures as a result of the north shift of the flames.

In all the tests, the expansion ratios of the fully expanded regions (Region 1) were about 30 and 25 for the waterborne and solvent-based intumescent coatings respectively, which are the same as those in the uniform ISO standard furnace tests [12, 24]. The expansion ratios of the expanding regions (Region 2) were approximately 20 and 15, respectively.

4.2 Cracking of intumescent coatings

Numerous cracks appeared on the surface of the coatings in all test specimens, which accords with prior observations of intumescent coatings applied on steel specimens [13, 24]. There were two

types of cracks, scattered narrow cracks perpendicular to the edges, and long cracks along the specimens at the corners of the cross-sections, as shown schematically in Figure 14. The crack locations tended to coincide with thermocouple locations, suggesting that the thermocouples may have acted as crack initiators, however this observation requires confirmation. The crack widths were typically between 2 and 6mm, with only a few cracks at the corners exceeding 10mm; these may be attributed to the intumescent coatings at the corners experiencing greater strains due to sharp changes in geometry in these regions.

Since most of the cracks were narrow and did not expose the steel surface, their influence on heat transfer and steel temperature is considered to be low [25]. To confirm this assertion, Figure 15 compares the measured steel temperatures at a crack location (i.e. Thermocouple TS-9-F, crack width 6mm) and at the nearby location without a local crack (i.e. Thermocouple TS-9-S1), both with similar adjacent gas phase temperatures, for the horizontal specimen with waterborne intumescent coatings. The steel temperatures are seen to be similar. The influence of any cracks on intumescent coating behaviour can be considered to be implicitly considered in the discussions that follow, which are based on measured steel temperatures.

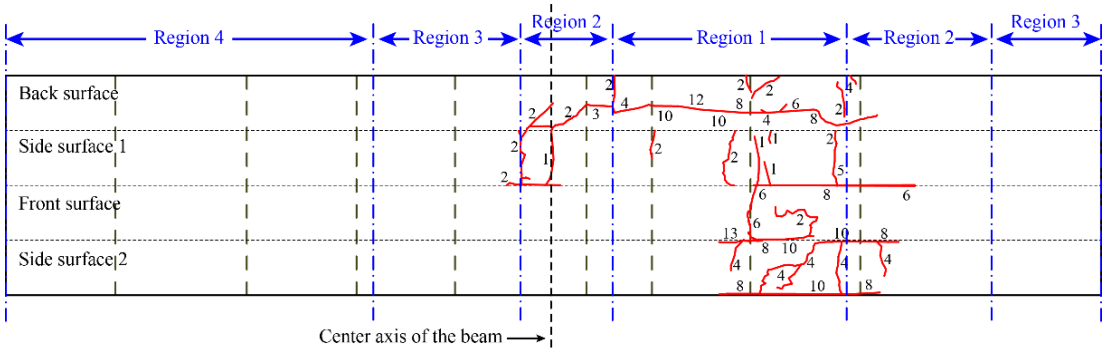

(a) BW

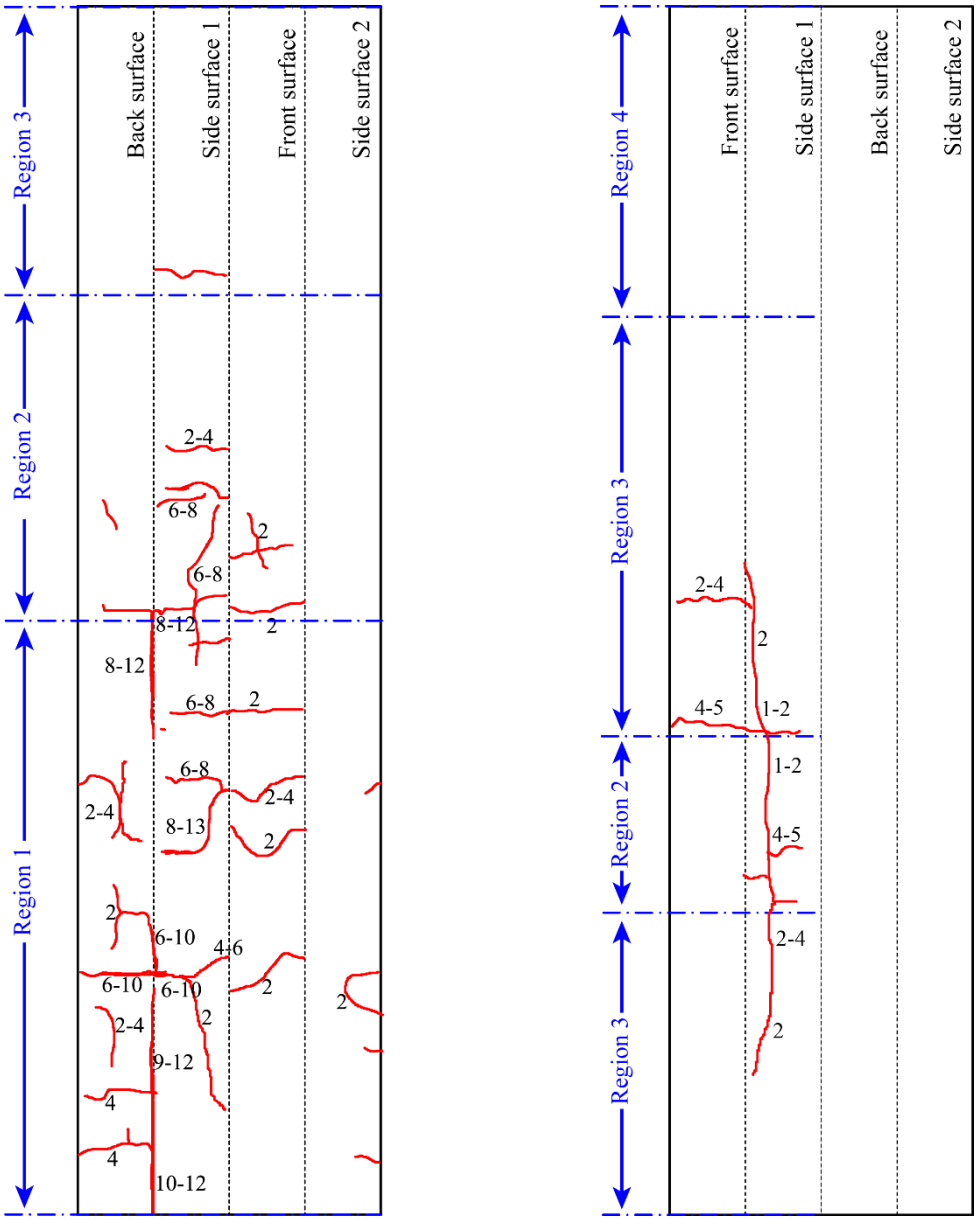

(b) CS1 (c) CW2

Figure 14 Typical distribution of cracks (numbers indicate crack width in mm)

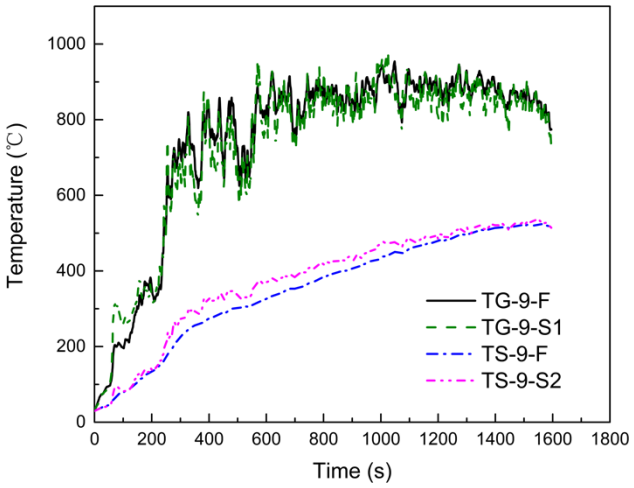

Figure 15 Comparison of measured steel temperatures with and without a local crack, BW

4.3 Expansion of intumescent coatings

Figures 16-21 show contours of the intumescent coating expansion ratio for the different specimens and relates them to average gas temperature distributions along the members during the steady burning periods of the experiments (i.e. 600-1400s). It can be seen that the full expansion regions (Region 1) coincide with the flame area. For the horizontal specimens, Region 2 (partially expanded region) were relatively small. In Region 3 (melted region), the expansion was very low. Therefore, when conducting heat transfer to the steel member, it may be possible to divide intumescent coatings approximately into two zones: the flame zone where the intumescent coatings achieve full expansion and the other zone where any expansion is negligible.

The average expansion ratios of the full expansion regions for the waterborne and solvent-based coatings were 29 and 21 respectively, and these were similar for the horizontal and vertical specimens. These expansion ratios agree with those for the same intumescent coatings in the authors' previous fire tests under the ISO 834 standard furnace testing conditions [12, 24]. This indicates that the same intumescent coatings have similar behaviour for the fully expanded regions under both uniform and spatially non-uniform (localised) heating conditions. This suggests that it may be

possible to assume the same thermal characteristics of intumescent coatings obtained from standard furnace test conditions, which are likely to be available from product development, to calculate steel temperatures to be expected under localised severe heating scenarios.

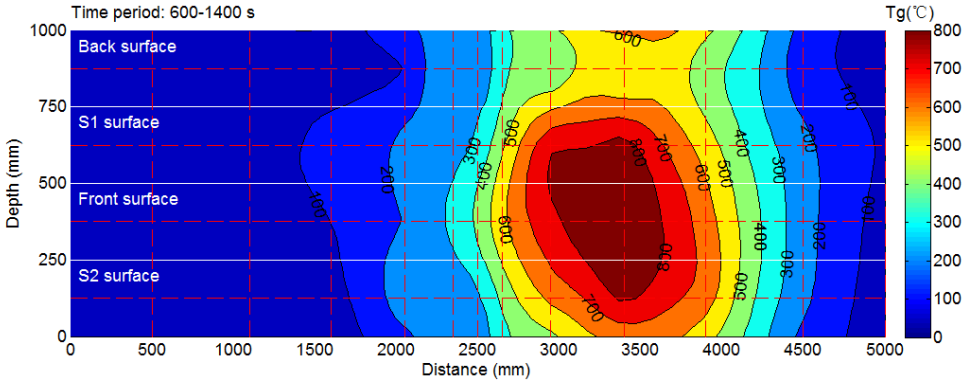

(a) Average gas temperature distribution

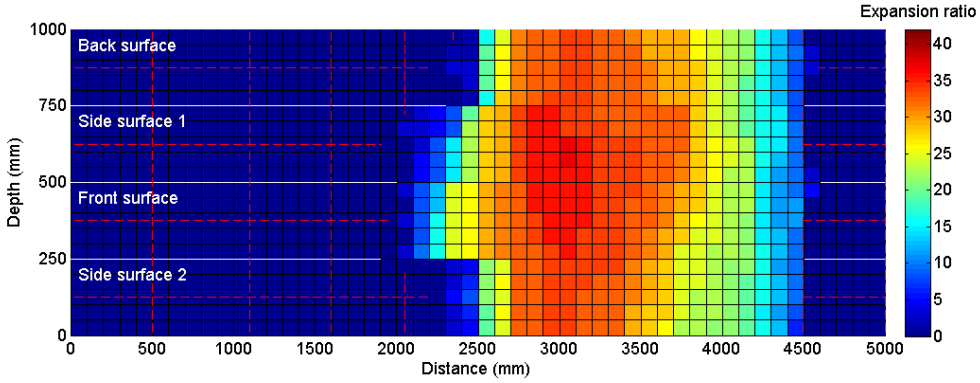

(b) Distribution of expansion ratios after fire

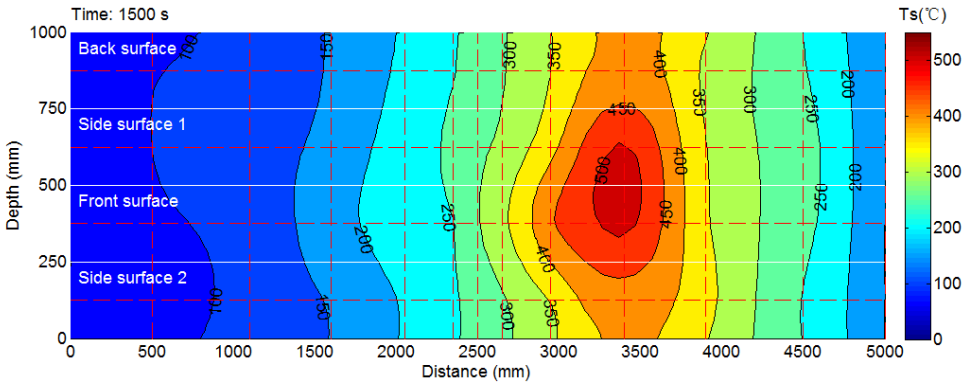

(c) Steel temperature distribution at 1500s

Figure 16 Horizontal specimen with waterborne intumescent coatings (BW)

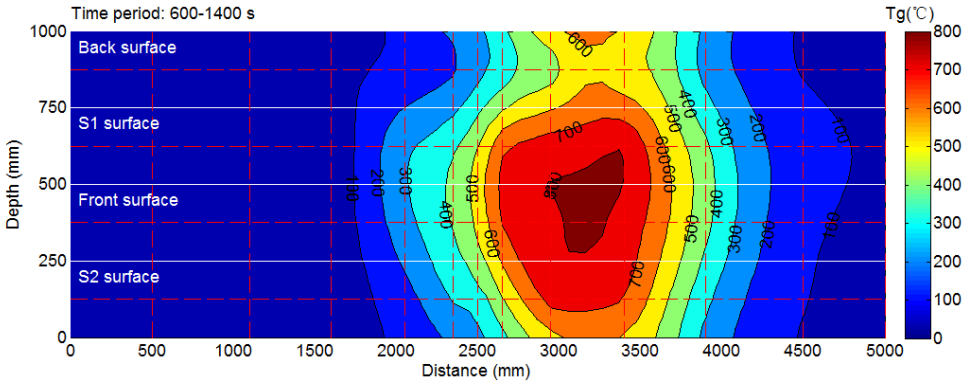

(a) Average gas temperature distribution

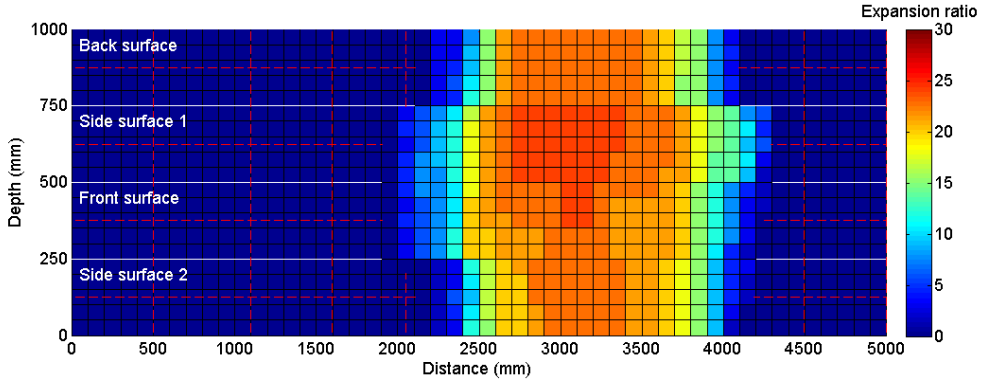

(b) Distribution of expansion ratios after fire

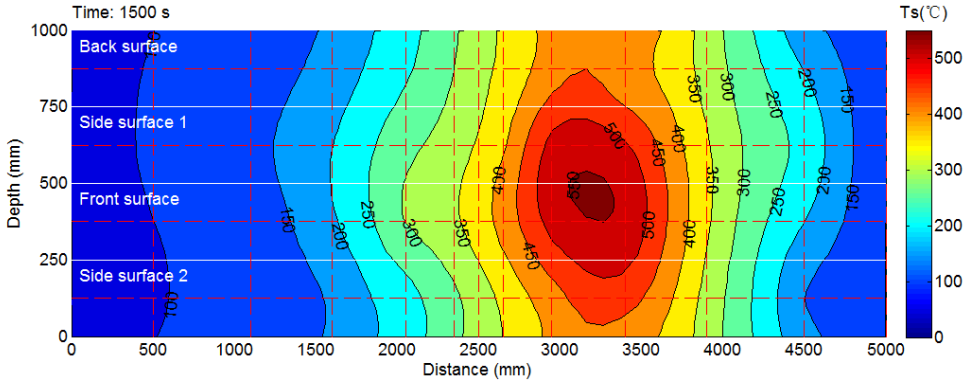

(c) Steel temperature distribution at 1500s

Figure 17 Horizontal specimen with solvent-based intumescent coatings (BS)

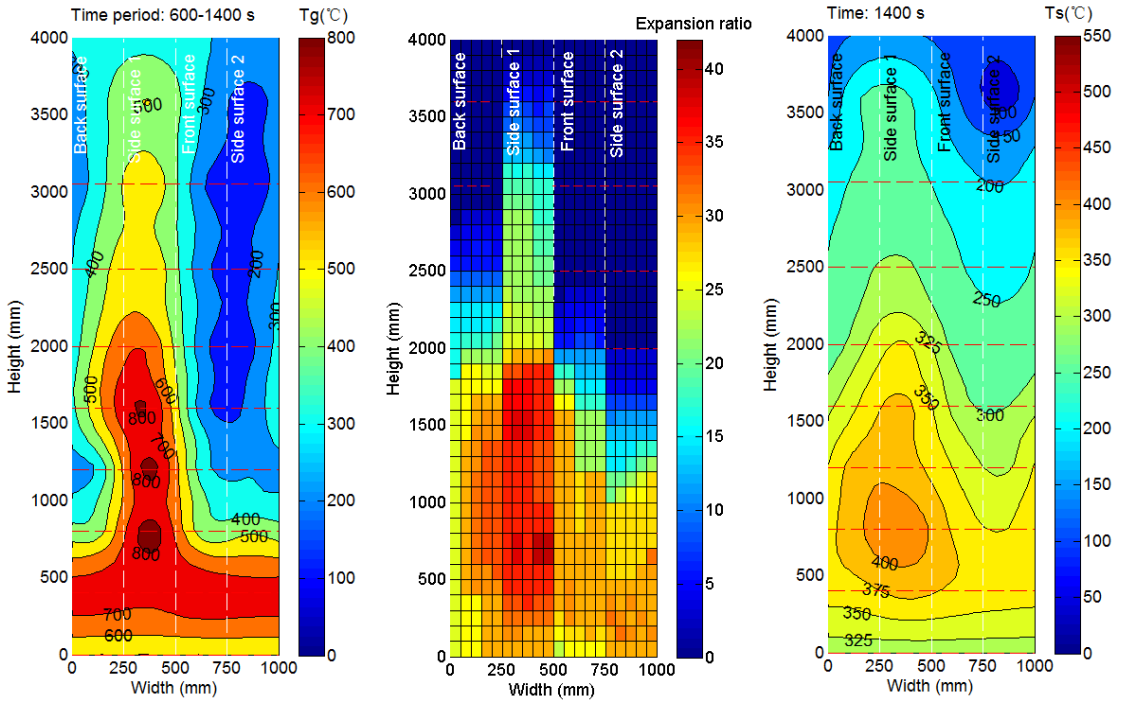

(a) Average gas temperature distribution (b) Distribution of expansion ratio after fire (c) Steel temperature distribution at 1500s

Figure 18 Vertical specimen with waterborne intumescent coatings, CW1

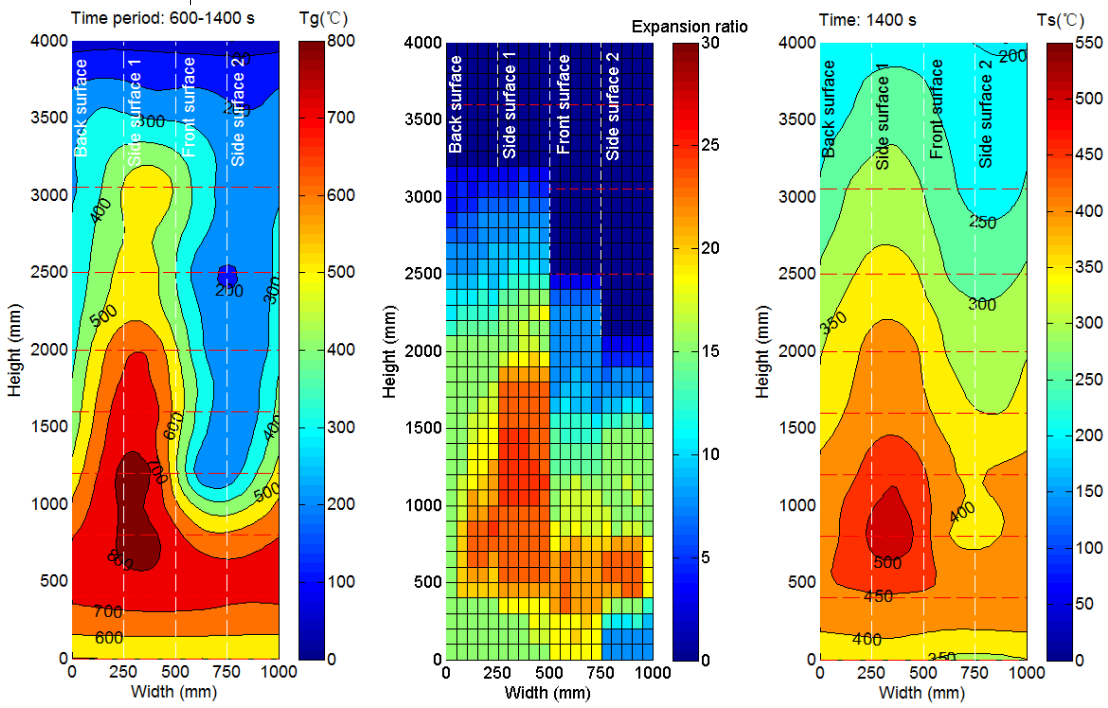

(a) Average gas temperature distribution (b) Distribution of expansion ratio after fire (c) Steel temperature distribution at 1500s

Figure 19 Vertical specimen with solvent-based intumescent coatings, CS1

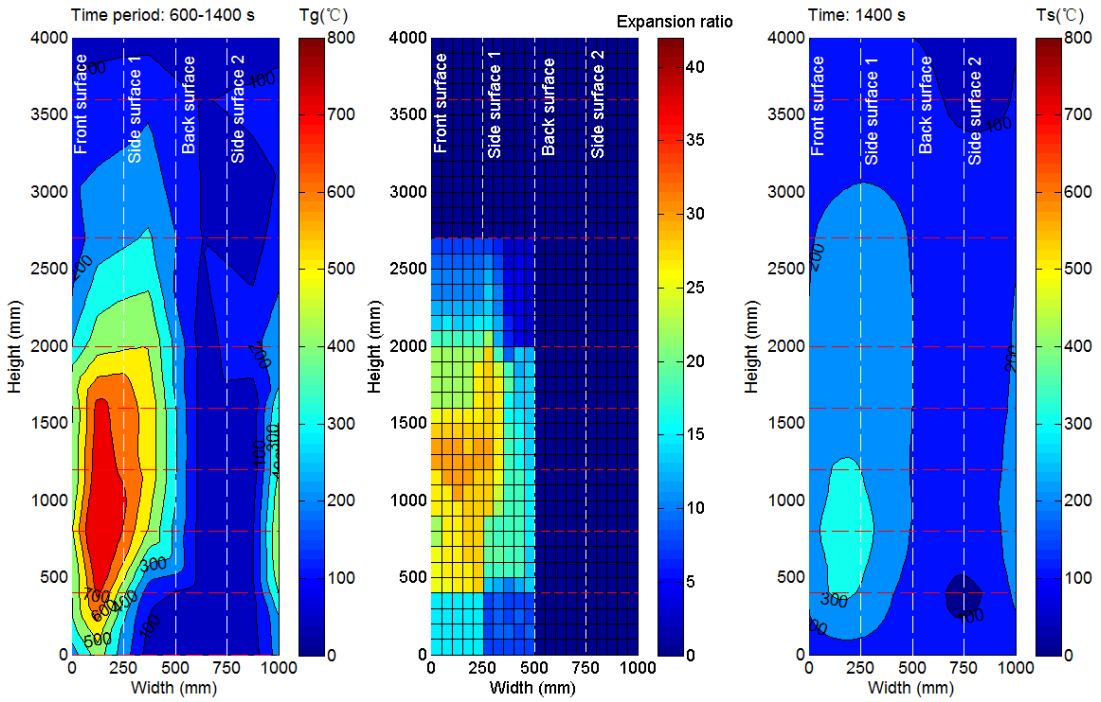

(a) Average gas temperature distribution (b) Distribution of expansion ratio after fire (c) Steel temperature distribution at 1500s

Figure 20 Vertical specimen with waterbone intumescent coatings, CW2

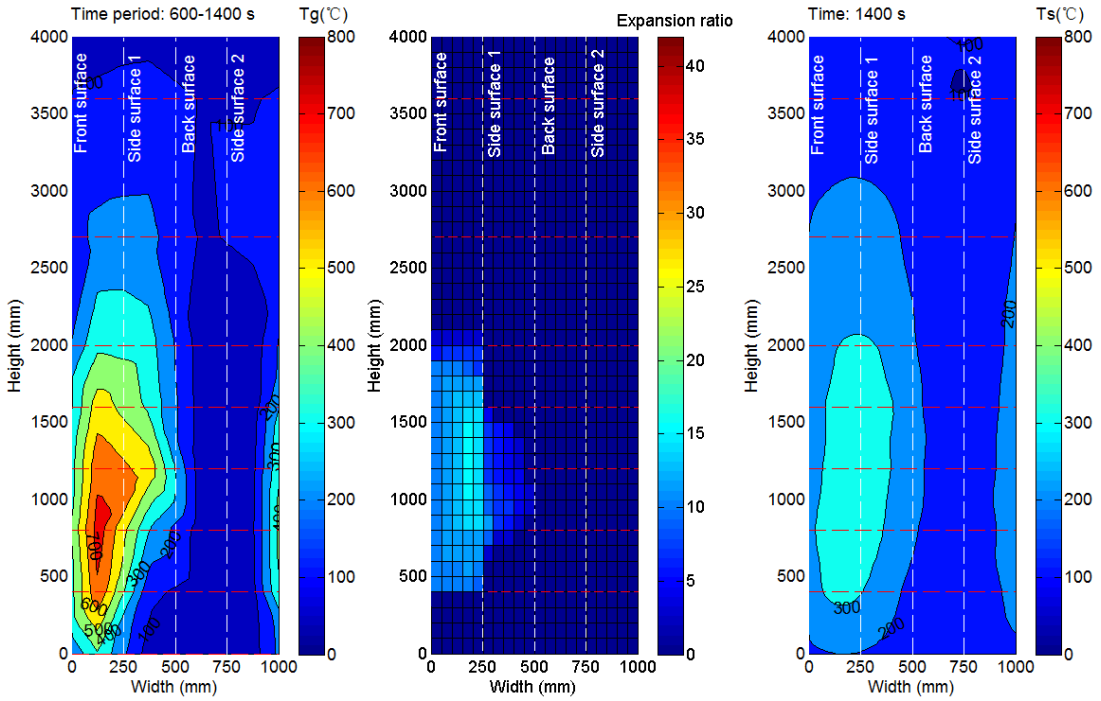

(a) Average gas temperature distribution (b) Distribution of expansion ratio after fire (c) Steel temperature distribution at 1500s

Figure 21 Vertical specimen with solvent-based intumescent coatings, CS2

5 STEEL TEMPERATURE DISTRIBUTIONS

Figures 16-21 present the maximum steel temperature contours for the horizontal and vertical specimens. Included in these figures are also intumescent coating expansion ratios and gas temperatures of the four regions of intumescent coatings described earlier. There are clear non-uniform steel temperature gradients in the cross-sections and along their length. The highest steel temperatures were in the expanded region (Region 1). However, due to longitudinal heat conduction, there were also moderate steel temperature rises (70℃-150℃) in regions where the intumescent coatings did not react. In general, the waterborne intumescent coating performed slightly better, with lower steel temperatures than solvent-based coating.

For the fully expanded regions (Region 1), the effective thermal conductivity of the intumescent coatings was calculated using the method in EN 13381-8 [14] – assuming that the intumescent coating's surface temperature was the same as the gas phase temperature and there was no heat conduction along the test specimens. This is given by:

$$\lambda(T_s) = d_p \rho_s c_s \frac{V}{A_p} \frac{\Delta T_s}{(T_g - T_s)\Delta t} \quad \textbf{(6)}$$

where A_p/V is the section factor of the steel member insulated by intumescent coatings; c_s is the temperature dependent specific heat of steel [J/kg K]; d_p is the initial dry film thickness of the intumescent coatings [m]; Δt is the time interval [s]; T_s is the steel temperature[K]; T_g is the fire temperature [K]; ΔT_s is the increase of fire temperature during the time interval Δt [K]; ρ_s is the density of steel [kg/m^3];

Figure 22 shows the temperature-dependent effective thermal conductivity curves, calculated by using Eqn. (6), for the fully expanded region for waterborne coating (BW-9-F) and solvent-based

coating (BS-9-F), together with the results of the previous ISO furnace tests [24] for the two types of intumescent coatings with same DFT. The comparison shows that the thermal conductivities of the expanding and full expansion stages for the fully expanded region under localized fires were close to that determined under the ISO standard temperature-time curve in a fire resistance testing furnace. The thermal conductivities of the melting stage under localized fires were different from those under the ISO standard fire. However, it is not important to achieve high accuracy in obtaining thermal conductivity for the first phase (100-300 °C) because the steel temperature is too low to affect the mechanical properties of steel. After the first phase, the steel temperature is higher, however, calculation of the steel temperature is mainly dependent on the thermal conductivities for the expanding and fully-expanded stages.

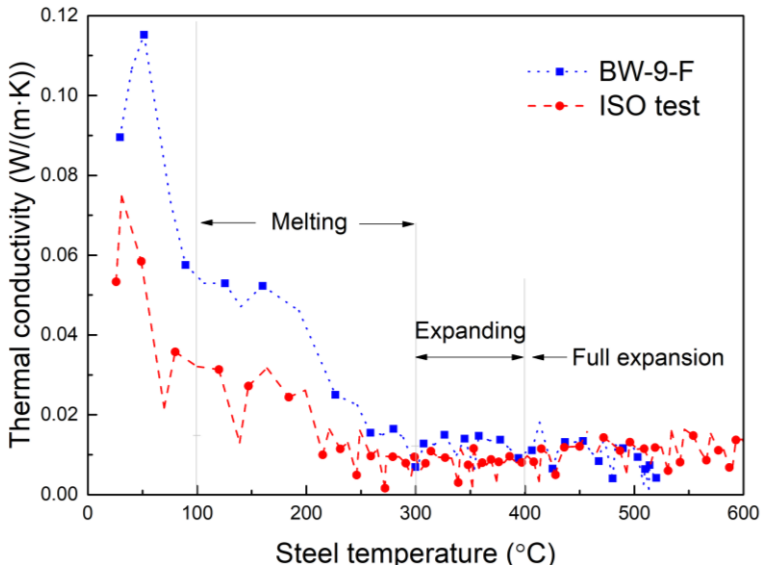

(a) Waterborne intumescent coatings

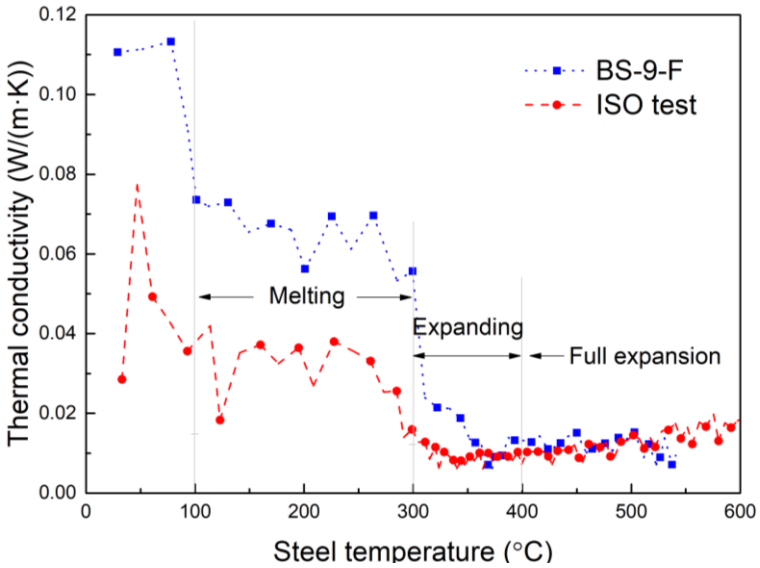

(b) Solvent-based intumescent coatings

Figure 22 Comparison of effective thermal conductivity-steel temperature curves for the full expanded region under localized fires and ISO fire

To validate the assertion that steel temperatures under localized heating can be calculated using the same thermal properties of intumescent coatings obtained from the ISO 834 standard furnace test condition, steel temperatures in the different regions of the test members were calculated using the three-stage effective thermal conductivity model obtained by the authors for the same intumescent coatings under standard ISO 834 furnace test conditions [13]. Figures 23 and 24 compare the calculated steel temperatures with those measured during the experiments presented herein.

The measured steel temperatures refer to those at the front surfaces of sections 11, 6, and 9 for waterborne intumescent coatings horizontal specimen (BW) and sections 4, 10, and 8 for solvent-based intumescent coating specimen (BS), which are in the center of the melting, expanding and full expansion regions, respectively. For these locations, it was assumed that the lumped mass method in Eurocode 3 Part 1.2 [26] can be used assuming limited heat transfer along the specimens.

In the steel temperature calculations, the thermal conductivities of intumescent coatings were

assumed to be constant for the melting, expanding and full expansion stages (corresponding to the steel temperature ranges of 100℃-300℃, 300℃-400℃ and above 400ºC, respectively), according to [13]. The effective thermal conductivities of the intumescent coatings for the fully expanded stage were the same as those obtained by the authors under the standard ISO 834 furnace test condition [24], being 0.012W/(m.K) and 0.014W/(m.K) respectively for the same type of waterborne and solvent-based intumescent coatings with the same DFT of 0.6mm. The ratio of effective thermal conductivity of the melting stage to that of the full expansion stage was taken as 4, and that for the expanding stage was taken as 0.5, according to [13].

Figure 23 and Figure 24 show that the calculated steel temperature results and the recorded steel temperatures are in reasonable agreement for different regions of the horizontal member (beam tests) for both types (waterborne and solvent-based) intumescent coatings. The relatively small differences, being less than 50 ºC for most locations, between the calculated and predicted steel temperatures may be attributed to ignoring heat conduction within the steel members in the simplified calculation method. This suggests that the same effective thermal conductivities for intumescent coatings obtained from testing under uniform heating conditions can be used to calculate steel temperatures in steel members under exposure to localized fires.

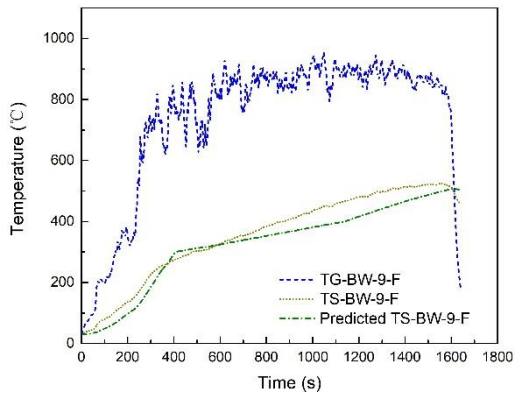

(a) Fully expanded region

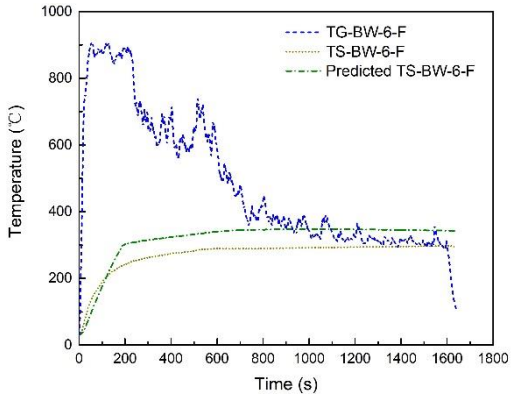

(b) Expanding region

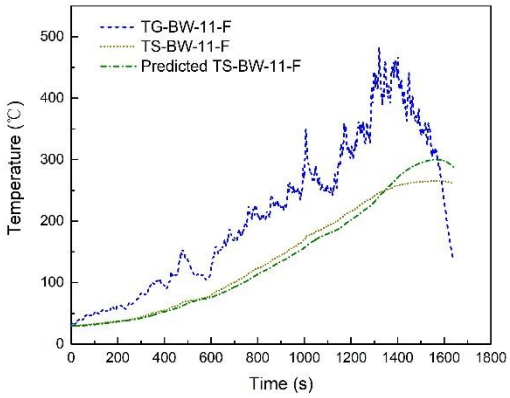

(c) Melting region

Figure 23 Comparison between predicted and measured steel temperatures, BW

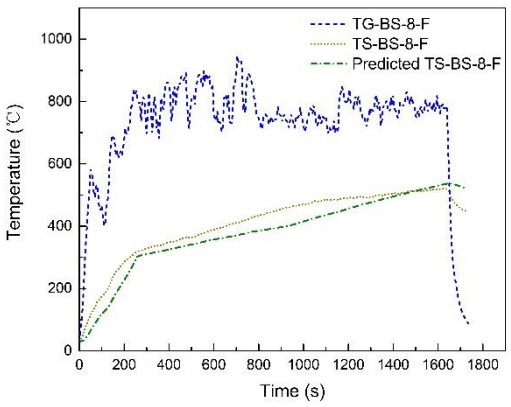

(a) Fully expanded region

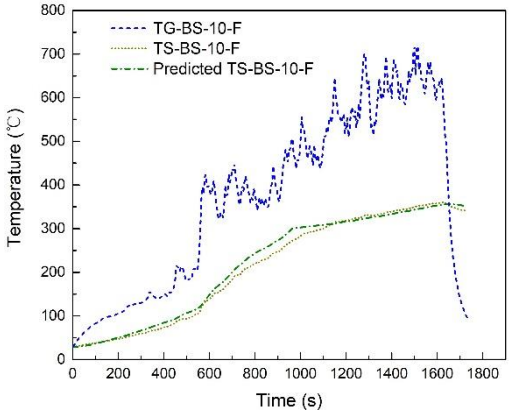

(b) Expanding region

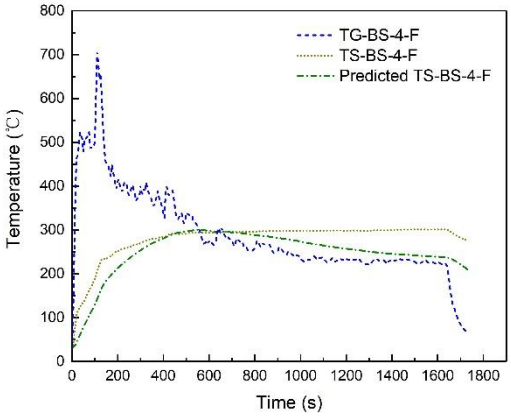

(c) Melting region

Figure 24 Comparison between predicted and measured steel temperatures, BS

6. CONCLUSIONS

This paper has presented the experimental results from a programme of fire tests to investigate the behaviour of intumescent coatings applied to steel hollow structural sections under localized fire exposures. This study has examined two types of intumescent coatings (waterborne and solvent-based) on horizontal and vertical specimens. Comparisons were made between the experimental results of this research, which deals specifically with localized fire exposure, and those under the ISO 834 standard furnace tests and non-standard furnace tests, as regards intumescent coating appearance after fire tests, expansion ratios, and steel temperatures. The main findings of this paper can be summarised as follows:

(1) Intumescent coatings at different locations of the horizontal and vertical specimens behaved differently because of the highly non-uniform thermal exposures experienced under exposure to localized fires. The behaviour of intumescent coatings can be approximately classified into four notional categories: (1) full expansion, (2) partially expanded, (3) melted but not expanded, and (4) essentially unreacted. The steel temperature ranges for these regions were approximately > 400°C, 300-400°C, 100-300°C, and less than 100°C, respectively; this is in agreement with observations under furnace test exposures for the specific coatings considered herein.

(2) The expansion ratios and constant thermal conductivities of the full expansion regions in the localised fire tests of this paper agree reasonably well with the results from furnace tests with uniform heating, once full expansion has been achieved (however the path to this condition

differed).

(3) Steel temperatures calculated using the three stage effective thermal conductivity model presented based on previous fire tests on the same intumescent coatings under uniform non-standard and standard ISO 834 furnace test conditions [13] were in reasonable agreement with the measured pool fire test results of steel temperatures from this research; the maximum difference being less than 50 ºC for most thermocouple locations.

(4) The thermal conductivity of the same intumescent coatings obtained under ISO 834 furnace test conditions can be reasonably applied to localised heating scenarios via the three stage thermal conductivity model proposed previously for uniform heating [13].

(5) Cracks, with widths in the range of 2-6mm, appeared on the surfaces of the intumescent coatings in the flame-exposed zone. These did not penetrate through the entire coating thickness to directly expose the steel surface. Therefore, their effects on steel temperature are not considered significant in the current context (as verified using data from the tests presented herein).

ACKNOWLEDGEMENTS

This study was supported by the Ministry of Science and Technology of China (SLDRCE14-A-05). The authors are grateful to the technicians of the Fire Safety of Engineering Structures Testing Division, part of the State Key Laboratory for Disaster Reduction in Civil Engineering of Tongji University, and the School of Engineering at the University of Edinburgh for their assistance with the fire tests and analysis. Intumescent coatings were supplied free of charge by a collaborating manufacturer.

REFERENCES

[1] BS EN 1991-1-2:2002. Eurocode 1: Actions on structures. Part 1-2: General actions – Actions on structures exposed to fire. BSI, London,

[2] Chao Zhang, John L. Gross, Therese P. McAllister, et al. Behaviour of Unrestrained and Restrained Bare Steel Columns Subjected to Localized Fire, J. Struct. Eng., 2015, 141(10).

[3] Daisuke Kamikawa, Yuji Hasemi, Takashi Wakamatsu, et al. Experimental flam heat transfer correlations for a steel column adjacent to and surrounded by a pool fire, Fire Saf. Sci.,2003, 7: 989-1000. doi:10.3801/IAFSS.FSS.7-989.

[4] Takashi Wakamatsu, Yuji Hasemi, Koji Kagiya, et al. Heating mechanism of unprotected steel beam installed beneath ceiling and exposed to a localized fire: verification using the real-scale experiment and effects of the smoke layer, Fire Saf. Sci., Proceedings of the seventh international symposium, pp. 1099-1110.

[5] Ferraz, G., Santiago, A., Rodrigues, J.P. et al. Thermal Analysis of Hollow Steel Columns Exposed to Localised Fires, Fire Technol (2016) 52: 663. https://doi.org/10.1007/s10694-015-0481-2.

[6] Alexandra Byström, Johan Sjöström, Ulf Wickström, David Lange, Milan Veljkovic, (2014) Large Scale Test on a Steel Column Exposed to Localized Fire, Journal of Structural Fire Engineering, Vol. 5 Issue: 2, pp.147-160, https://doi.org/10.1260/2040-2317.5.2.147.

[7] François Hanus, Olivier Vassart, Nicola Tondini, et al. Temperature assessment of a vertical steel member subjected to localised fire: Experimental tests. Proceedings of the 10th International Conference of Structure in Fire. 2018.

[8] NIST Technical Note 1983: National Fire Research Laboratory Commissioning Project: Testing Steel Beams under Localized Fire Exposure. NIST. https://doi.org/10.6028/NIST.TN.1983

[9] Tondini N., Thauvoye C., Hanus F.H., et al., Development of an analytical model to predict the radiative heat flux to a vertical element due to a localized fire. Fire Saf. J., 2019, 105: 227-243.

[10] M. Jimenez, S. Duquesne, S. Bourbigot, Characterization of the performance of an intumescent fire protective coating. Surf. Coat. Technol.,2006, 201(3-4):979–987.

[11] G.Q. Li, G.B. Lou, C. Zhang, et al., Assess the fire resistance of intumescent coatings by equivalent constant thermal resistance, Fire Technol. 48 (2012) 529–546.

[12] G. Q. Li, J. Han, Y. C. Wang, Constant effective thermal conductivity of intumescent coatings: analysis of experimental results. J. Fire Sci., 2017, 35(2):132-155.

[13] J. Han, G.Q. Li, Y.C. Wang, Q. Xu, An experimental study to assess the feasibility of a three stage thermal conductivity model for intumescent coatings in large space fires, *Fire Safety Journal* (2019), doi: https://doi.org/10.1016/j.firesaf.2019.102860.

[14] BS EN 13381-8. Test methods for determining the contribution to the fire resistance of structural members, Applied reactive protection to steel members, BSI, London, 2013.

[15] L. Wang, Y. Dong, C. Zhang et al. Experimental study of heat transfer in intumescent coatings exposed to non-standard furnace curves, Fire Technol., 51(3), 627-643.

[16] A. Elliott, A. Temple, C. Maluk et al. Novel testing to study the performance of intumescent coatings under non-standard heating regimes, Fire Safety Science-Proceedings of the eleventh international symposium, 2014, 652-665.

[17] A. Lucherini, L. Giuliani, G. Jomaas. Experimental study of the performance of intumescent coatings exposed to standard and non-standard fire conditions, Fire Saf. J., 2018, 95, 42-50.

[18] D. de Silva, A. Bilotta, E. Nigro, Experimental investigation on steel elements protected with intumescent coating, CONSTR. BUILD. MATER. 2019, 205: 232-244. https://doi.org/10.1016/j.conbuildmat.2019.01.223.

[19] D. de Silva, A. Bilotta, E. Nigro, Effect of the thermal input on the behavior of intumescent coatings, Proceedings of the International Conference of Applications of Structural Fire Engineering (ASFE 2017), Manchester, United Kingdom.

[20] Babrauskas, V. Heat release rates, SFPE Handbook of Fire Protection Engineering. Section 26, 5th ed. Society of Fire Protection Engineers, Maryland, USA.

[21] Hostikka S, Kokkala M, Vaari J. Experimental study of the localized room fires. NFSC2 test series (VTT building technology) VTT research notes 2104; 2001.

[22] Heskestad G. Fire plumes, flame height, and air entrainment. SFPE Handbook of Fire Protection Engineering. Section 13, 5th ed. Society of Fire Protection Engineers, Maryland, USA.

[23] Griffin, G. J. (2010). The Modeling of Heat Transfer across Intumescent Polymer Coatings. Journal of Fire Sciences, 28(3), 249–277.

[24] Xu Q., Li G. Q., Jiang J., et al., Experimental study of the influence of topcoat on insulation performance of intumescent coatings for steel structures. Fire Saf. J., 2018, 101: 25-38.

[25] Wang J. Effect of local damage of fire insulation on temperature distribution of steel members subjected to fire (Master's thesis). Tongji University, Shanghai, 2006.

[26] BS EN 1993-1-2:2005. Eurocode 3: Design of steel structures — Part 1-2: General rules — Structural fire design. BSI, London, 2005.